

Ventilation Processes in a Three-Dimensional Street Canyon

Štěpán Nosek¹ · Libor Kukačka² ·
Radka Kellnerová¹ · Klára Jurčáková¹ · Zbyněk Jaňour¹

Received: 8 July 2015 / Accepted: 14 January 2016 / Published online: 1 February 2016
© Springer Science+Business Media Dordrecht 2016

Abstract The ventilation processes in three different street canyons of variable roof geometry were investigated in a wind tunnel using a ground-level line source. All three street canyons were part of an urban-type array formed by courtyard-type buildings with pitched roofs. A constant roof height was used in the first case, while a variable roof height along the leeward or windward walls was simulated in the two other cases. All street-canyon models were exposed to a neutrally stratified flow with two approaching wind directions, perpendicular and oblique. The complexity of the flow and dispersion within the canyons of variable roof height was demonstrated for both wind directions. The relative pollutant removals and spatially-averaged concentrations within the canyons revealed that the model with constant roof height has higher re-emissions than models with variable roof heights. The nomenclature for the ventilation processes according to quadrant analysis of the pollutant flux was introduced. The venting of polluted air (positive fluctuations of both concentration and velocity) from the canyon increased when the wind direction changed from perpendicular to oblique, irrespective of the studied canyon model. Strong correlations (>0.5) between coherent structures and ventilation processes were found at roof level, irrespective of the canyon model and wind direction. This supports the idea that sweep and ejection events of momentum bring clean air in and detrain the polluted air from the street canyon, respectively.

Keywords Coherent structures · Line source · Pollution flux measurements · Street canyon · Wind tunnel

✉ Štěpán Nosek
nosek@it.cas.cz

¹ Institute of Thermomechanics of the CAS, v. v. i., Dolejškova 1402/5, Prague, Czech Republic

² Faculty of Mathematics and Physics, Department of Meteorology and Environment Protection, Charles University in Prague, V Holešovičkách 2, Prague, Czech Republic

1 Introduction

Street canyons are of research interest because they have the highest concentrations of pollutants in cities. Because of the geometric complexity of buildings and transitional meteorological conditions, dispersion processes within street canyons are complex. Extensive wind-tunnel (e.g., Meroney et al. 1996; Rafailidis 1997; Kastner-Klein et al. 2004; Perret and Savory 2013; Addepalli and Pardyjak 2014; Carpentieri and Robins 2015) and computational fluid dynamics (CFD) studies (e.g., Leidl and Meroney 1997; Baik and Kim 2002; Xie et al. 2005; Madalozzo et al. 2014; Huang et al. 2015) have been performed over the last three decades to clarify these dispersion processes. Compared with field measurements (e.g., Louka et al. 2000; Nelson et al. 2007; Zajic et al. 2015), physical modelling using a wind tunnel is more favourable in terms of the cost and ability to control input variables (Schatzmann and Leidl 2011). Despite the increasing use of CFD simulation for the prediction of flow and pollutant dispersion within the urban canopy layer, there is still the need to validate such simulation with experimental data (Blocken 2015).

The ideally modelled street canyon is a two-dimensional (2D) rectangular cavity exposed to fully turbulent flow. If the flow is perpendicular to a canyon having an aspect ratio of near unity (H/B , where H is the building height and B is the canyon width), a strong shear layer develops across the top of the cavity (Perret and Savory 2013; Savory et al. 2013). Owing to the unstable flow condition, the shear layer intermittently flaps up and down and is affected by fluxes of turbulent kinetic energy from the external flow as observed by Salizzoni et al. (2011). The phenomena of these unstable dynamics were also observed by Louka et al. (2000) in a field experiment performed between two long bars with pitched roofs. Inside the cavity there develops a vortex that has a rotation axis parallel to the street and is neither steady nor symmetric (Britten and Hanna 2003) and is sensitive to changes in the structure of the external flow (Salizzoni et al. 2011). A strong channel effect arises for airflow that is parallel with the canyon, where the pollutants are transported predominantly by horizontal advection. A helical vortex along the canyon dominates for the oblique wind direction (Belcher 2005).

However, the real street canyon is part of a city street network with intersections, and three-dimensional (3D) street canyons of finite length incorporated in an urban-like array are thus more appropriate to model (Klein et al. 2007; Carpentieri and Robins 2015). The morphology of a real street canyon usually comprises uneven roof heights along one or both sides of the canyon (i.e., the so-called non-uniform street canyon, as introduced by Gu et al. (2011)). This morphology provides additional openings for flow aloft to penetrate the canyon and to produce structures that are more complex than the along-canyon vortex, which typically forms for idealized quasi two-dimensional uniform street canyons. Both wind-tunnel (Klein et al. 2007) and field (Nelson et al. 2007) studies have demonstrated the importance of building-height variability along both street sides on canyon-flow dynamics and pollutant dispersion. More recently, a CFD study (Gu et al. 2011) employing a large-eddy simulation (LES) model was conducted for simplified variations of non-uniform street canyons and revealed new flow features, such as the tilting of flow streamlines and the horizontal divergence and convergence of airflow inside and just above the canyon. The simulation of pollutant concentrations using a line source at the centre of the canyon revealed that uneven building heights enhance pollutant dispersion through large-scale exchange of air mass inside and above such non-uniform canyons.

Perret and Savory (2013) and more recently Carpentieri and Robins (2015) highlighted two main approaches used in previous wind-tunnel studies to observe the effects of urban morphology on flow and dispersion in cities. The first approach (e.g., Dabberdt 1991; Kastner-

Klein and Plate 1999; Baik et al. 2000; Robins et al. 2002; Perret and Savory 2013; Addepalli and Pardyjak 2014) concerns directly the flow characteristics inside the street canyon and is mainly based on local canyon geometric parameters, such as the building and canyon aspect ratios (H/B and H/L , respectively, where L is the canyon length). The second approach (e.g., Grimmond and Oke 1999; Cheng and Castro 2002; Takimoto et al. 2013; Blackman et al. 2015) is related to boundary-layer parameters (i.e., aerodynamic roughness length, z_0 , friction velocity, u_*) or larger-scale geometrical characteristics of the urban models, such as the mean building height (h_m) or the plan-area index ($\lambda_p = A_b/A_t$, where A_b is the area occupied by the buildings and A_t is the total ground area) or the frontal area index ($\lambda_f = A_f/A_t$, where A_f is the frontal area of the buildings viewed from the approach direction of flow). While the second approach might be sufficient for the parametrization of the flow inside the canyon to some extent, local geometrical features affect local wind profiles within the canyons more strongly (especially in 3D cases) than larger-scale geometrical characteristics (Carpentieri and Robins 2015). Hence, the present study takes the first approach in examining the effect of the aforementioned building-height non-uniformity on local pollutant dispersion within the 3D street canyon under neutral stability. The following review is of wind-tunnel studies that have taken the first approach, except where stated otherwise.

Since the 1970s, 3D street-canyon arrangements, including a line source, have been investigated in many wind-tunnel studies with respect to the mean velocity and concentration fields and neutrally-stratified conditions. Hoydysh et al. (1974) pointed out that a high-density configuration of uniformly sized buildings generally increases pollutant concentrations, whereas a configuration with varying building heights allows pollutants to escape. Another important conclusion of that work was that the pair of vertical vortices emerging at street corners transports less polluted air into the street compared with the case for 2D street canyons. The leeward concentration in the middle of the canyon thus increases with increasing canyon length.

Hoydysh and Dabberdt (1988) studied the effects of different set-ups of asymmetric street canyons (with the upwind building having a different height than the downwind building, but both having constant height along the canyon length) and wind direction (varying from 0 to ± 90 deg in 10 deg increments) on the street-canyon concentration. For step-up street-canyon types ($H_U < H_D$, where H_U and H_D are the heights of the upwind and downwind buildings, respectively), the concentration levels at the leeward wall were at least twice those at the windward wall. The opposite phenomenon occurred for a step-down ($H_U > H_D$) configuration; i.e., the concentration at the windward wall was slightly higher than that at the leeward wall. Generally, the concentrations in a step-up canyon were half those in a symmetric or step-down canyon. The detailed flow patterns inside quasi-2D asymmetric canyons having three different building aspect ratios were studied by Baik et al. (2000) in a water channel. The magnitudes of the updraft and downdraft were almost independent of the aspect ratio (H/B). One vortex was observed within the canyon in the case of a step-up building arrangement while two counter-rotating vortices were observed within the canyon for a step-down building arrangement.

Theurer (1999) summarized results from several wind-tunnel studies and found that the local concentration within the street canyon is a function of the wind direction, the vehicle-induced turbulence and the local building arrangement, providing neutral atmospheric stability. Here, the building arrangement refers to the building and canyon aspect ratios (H/B and L/H , respectively), the distance from the centre of the vehicle lanes to the building walls (assumed to be $B/2$ for a symmetric arrangement of the vehicle lanes), roof types and surroundings. Despite the different input conditions, such as the approach flow, scale, dimensions and position of the source, each study showed that the concentration increases

with increasing H/B . The same was found for the canyon length, confirming the results of the previously mentioned [Hoydysh et al. \(1974\)](#). The roof shape had a weaker but still important effect on the pollutant concentration in street canyons. For $H/B = 1$, the concentration at the leeward side of canyons with pitched roofs was approximately 30 % lower than those with flat roofs ([Rafailidis and Schatzmann 1995](#)). Later, [Rafailidis \(1997\)](#) suggested that altering the roof shape might have a stronger beneficial effect than increasing the spacing between buildings on urban air quality.

A systematic wind-tunnel study of parameter (L/H , B/H , upwind building presence, roof shape and wind direction) variations affecting the mean concentration profiles along leeward and windward two-dimensional street-canyon walls was performed by [Kastner-Klein and Plate \(1999\)](#). Vehicle emissions were simulated as two ground-level line sources positioned equidistantly from the centre of the investigated street canyon. In good agreement with the results of previous studies, the reduction of L/H led to a 3D flow pattern that decreased the mean concentration; the presence of additional upwind buildings increased the mean concentration inside the canyon; and the mean concentration decreased with the wind direction changing from perpendicular to oblique. In a later study, [Kastner-Klein et al. \(2004\)](#) demonstrated for a detailed reconstructed urban landscape model (of central Nantes, France) the important effect of the roof shape on flow and dispersion within the canyon. The main conclusion was that it is necessary to model a real array of buildings to obtain results that are realistic.

To better understand street-canyon ventilation processes, pollution flux exchanges have studied experimentally ([Barlow et al. 2004](#); [Carpentieri et al. 2012](#); [Kukacka et al. 2014](#)) but foremost numerically (e.g., [Baik and Kim 2002](#); [Liu et al. 2005](#); [Yang and Shao 2008](#); [Cai et al. 2008](#); [Liu et al. 2015](#)) owing to difficulties in simultaneously measuring velocity and the pollutant concentration. CFD studies have mainly focused on quasi 2D canyons, where scalar exchange rates provide a mass flux equilibrium between the canyon cavity and free surface layer above the canyon that is simpler than that observed in more complex 3D cases ([Nozu and Tamura 2012](#); [Michioka et al. 2014](#); [Moon et al. 2014](#)). While simplified, the numerical simulation of these 2D cases gave important answers to problems of ventilation and pollutant removal processes with respect to different street-canyon aspect ratios and morphologies of roof shapes or canyon-height asymmetry. The pollutant removal from a 2D canyon at roof level is mainly driven by the turbulent transport mechanism and the mean flow aids the pollutants to re-enter the street-canyon cavity ([Baik and Kim 2002](#)). [Liu et al. \(2005\)](#) showed that a cavity having a unity aspect ratio ($H/B = 1$) has a higher pollutant exchange rate (defined as the ratio of the turbulent vertical pollution flux to the rate of pollutant emission from the source) than a cavity having $H/B = 0.5$ or 2. His main conclusion was that complex turbulent transport cannot be represented by a simple gradient diffusion model. More recently, [Liu et al. \(2015\)](#) demonstrated for 2D canyons having different hypothetical building morphologies that, whereas the air exchange rate of the canyons had a strong linear relationship with the square root of the friction factor for all tested building morphologies, the turbulent pollutant flux correlated loosely. They pointed out that additional LES and experimental studies are needed to examine the detailed flow physics and pollutant removal mechanism over 3D urban areas.

To our knowledge, since the work of [Carpentieri et al. \(2012\)](#) addressed street intersections in the implicit study of street canyons, there has been only one wind-tunnel study ([Kukacka et al. 2014](#)) on both advective and turbulent pollution transport within a 3D street canyon. That study concluded that a strong recirculation vortex brought about intensive advective pollution flux at the mid-height of the street canyon ($H/B = 1.25$, $L/H = 4.8$, formed by courtyard buildings with a pitched roof), whereas at roof level, a higher contribution of the turbulent

pollution flux to the total was observed. The turbulent pollution transport was opposite to advective at the mid-height of the canyon, but at roof level both transport mechanism had the same (upward) direction. Similar phenomena were observed by [Michioka et al. \(2014\)](#) using an LES model for 3D street canyons with almost the same aspect ratios ($H/B = 1$, $L/H = 4$) and a ground-level line source.

Interestingly, there has been a lack of systematic wind-tunnel studies on pollutant transport within 3D street canyons, where the upwind or downwind buildings (or both upwind and downwind buildings) have a variable roof height along the canyon spanwise direction. The flow within the street canyon is mainly affected by the architecture and arrangement of buildings, and the spatial variability of the roof height and shape should be of primary concern, as was demonstrated in the aforementioned studies. For a better understanding of the effects of the 3D non-uniformity of a street canyon on ventilation processes, and to provide additional experimental data for CFD models, we here present an extension of our previous work ([Kukacka et al. 2014](#)). The extension principally refers to the effects of two parameters, the approach wind direction and pitched-roof height non-uniformity in all directions (thus considering a 3D street canyon), on pollutant transport within a 3D street canyon. This requires not only the mean flow and concentration fields but also the vertical pollution fluxes (turbulent and mean) and coherent structure analysis in two horizontal planes, namely at the mid-height of the canyon and at roof level.

2 Methods

2.1 Street-Canyon Models

Typical patterns of street canyons in the centres of Central European cities were used as the initial designs of three types of 3D street-canyon models having a scale of 1:400 (Fig. 1). All designed canyon models (labelled M1, M2 and M3) were a part of an urban-like array with a constant street width ($B = 50$ mm) formed by 8×4 courtyard-type buildings of constant length ($L = 300$ mm) and width ($B_B = 150$ mm) (Fig. 1c).

The first canyon model (M1), considered as the reference model, was part of an urban-like array (A1) with courtyard-type buildings having the same roof height $H = 62.5$ mm (Fig. 1d). Model M1 therefore has constant building and canyon aspect ratios ($H/B = 1.25$ and $L/H = 4.8$, respectively). To check the similarity of flow, we examined two M1 models, where $M1_R$ and $M1_L$ were positioned on the right and left of the streamwise avenue, respectively, and in the fourth row (in the streamwise direction) of the urban array (Fig. 1c). This position has been shown to be representative with respect to flow regime independence in many wind-tunnel studies (e.g., [Bezpalcova 2006](#)).

For the examination of fully 3D street-canyon ventilation processes, we designed the second urban model (A2) according to the same plan dimensions of model A1 (corresponding to the same plan area index, $\lambda_{pA1} = \lambda_{pA2} = 0.43$), but with arbitrarily varying roof heights along each canyon wall in the spanwise direction. However, the mean height of the urban-like array A2, h_{A2} , corresponded to the mean height of the urban-like array A1, h_{A1} , and hence $h_{A2} = h_{A1} = H$. The second (M2) and third (M3) canyon models were situated at the same positions as models $M1_R$ and $M1_L$, respectively (Fig. 1c). While street-canyon model M2 represents locally two step-up and two equally high roof configurations, model M3 represents two step-downs, one step-up and one equally high roof configuration (Fig. 1b). The local configurations for both canyon models were distributed randomly.

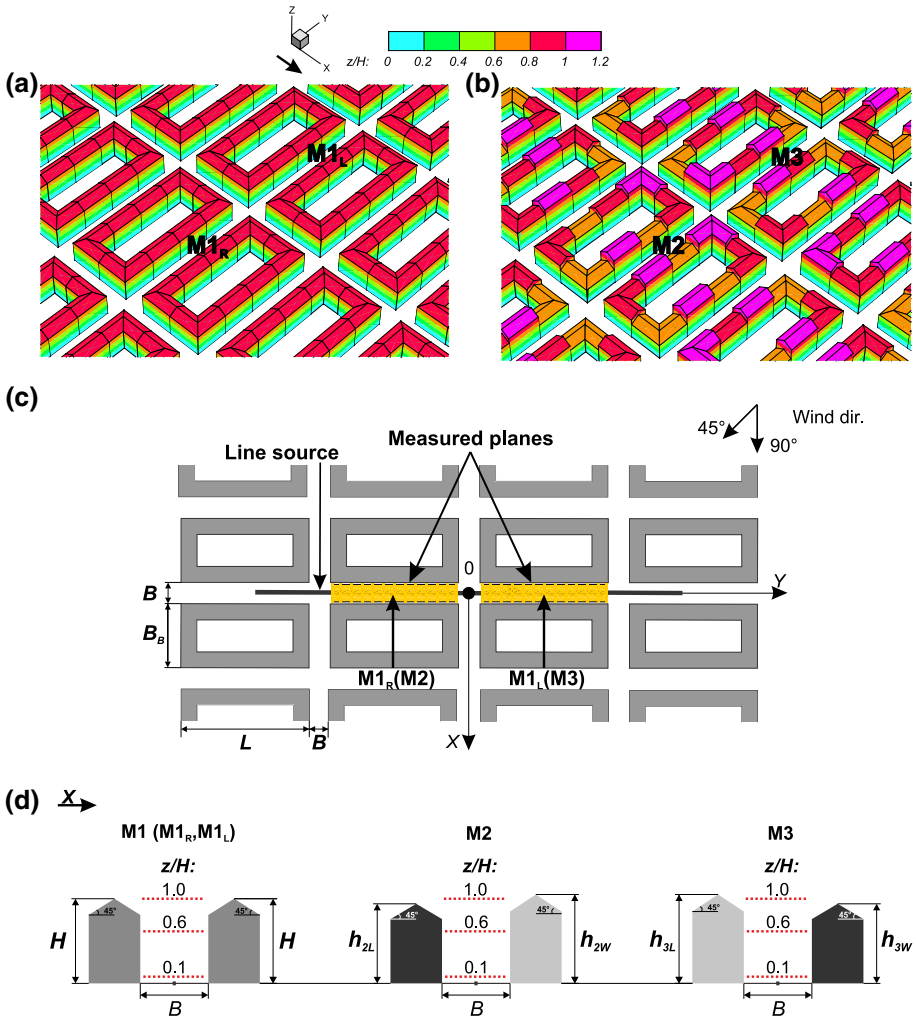


Fig. 1 Schemas of the models with respect to wind-tunnel coordinates x, y, z : isometric view of the urban-like array **a** A1, incorporating the street-canyon models $M1_R$ and $M1_L$, and **b** A2, incorporating the street-canyon models $M2$ and $M3$; **c** top view of the horizontal cross-sections of the two urban models (A1 and A2) at dimensionless height $z/H = 0.6$ with the measured horizontal planes (yellow rectangles) and origin of the coordinates; **d** side view of the measured horizontal planes (z/H) within the street-canyon models $M1, M2$ and $M3$ (where, for canyons $M2$ and $M3$, the projections of the mean building heights along the leeward (h_L) and windward (h_W) canyon walls are used)

Because of the roof height non-uniformity along the each side of the modelled canyons, we introduced the mean building aspect ratio of the canyon; e.g., $h_{2L}/B = 1.18$ and $h_{2W}/B = 1.31$ are the ratios of the mean building heights along the leeward and windward walls to the canyon width of the model $M2$, respectively. Similarly, for model $M3$, $h_{3L}/B = 1.31$ and $h_{3W}/B = 1.18$ (Fig. 1d). Hence, from an integral point of view, canyon model $M2$ can be classified as a step-up canyon and model $M3$ as a step-down canyon.

We simulated two approach wind directions for both urban-array models. The first direction was perpendicular to the street canyons while the second was oblique (45°) to the street canyons (Fig. 1c). We did not observe any appreciable wind-tunnel side effects on the flow

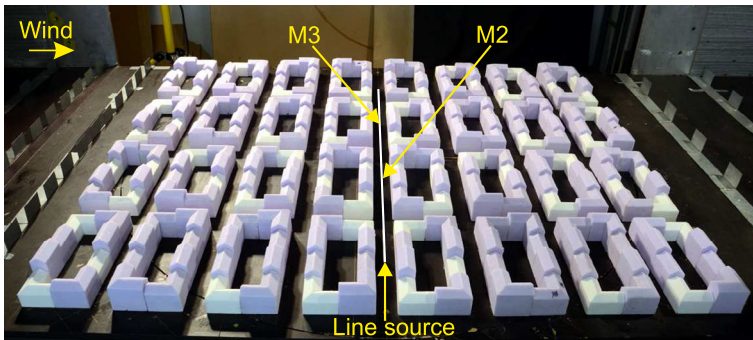


Fig. 2 Photograph of the urban-like array model A2 positioned at the bottom of the wind tunnel for the perpendicular wind direction. The flow is from *left to right* and the line source is positioned in the middle of the model and investigated street canyons M2 and M3

above the investigated street canyons for either simulated direction in lateral flow homogeneity tests at three different heights ($z/H = 2, 4$ and 6). The standard error of the mean streamwise velocity component was lower than 1.7% for all investigated points (where the velocity measurement error was 1%). As one example from four wind-tunnel runs, a photograph of the urban array model A2 positioned at the bottom of the wind tunnel for the perpendicular wind direction is presented in Fig. 2.

2.2 Line-Source Model

To simulate the pollution emitted by dense traffic within the street canyon, we designed a homogenous ground-level line source of a passive tracer gas (ethane in our case) according to Meroney et al. (1996). The total length of the line source was $L = 1$ m (400 m at full scale) and the line source ran continuously through the investigated street canyons (Fig. 1c). The line source was formed by a line of 504 equally spaced tubes made of stainless steel. The tubes had an inner diameter of 0.3 mm and length of 100 mm. The pressure drop across the tubes ($\Delta p_n = 64.5$ Pa) was sufficiently higher than the highest expected pressure fluctuations (up to 10 Pa) at the bottom of the wind tunnel, thus providing a stable volume flow rate (Meroney et al. 1996).

The lateral homogeneity of the line source was verified in several measuring and visualization tests. The standard error of the mean concentration measured along the entire source length at dimensionless downstream position $x/H = 1$ from the source (without the model) was lower than 5% (where the concentration measurement error was 4%). The ethane volume rate of flow from the line source was established in flow-rate independence tests for $Q = 18$ ml s^{-1} , at a wind-tunnel freestream velocity $U_0 = 6.2$ m s^{-1} . The computed velocity magnitude of the trace gas discharge from the line source was 0.28 m s^{-1} , which was significantly lower than the friction velocity ($u_* = 0.43$ m s^{-1}) of the canyons.

2.3 Experimental Set-Up

2.3.1 Wind Tunnel

We used the open low-speed environmental wind tunnel of the Institute of Thermomechanics of the Czech Academy of Sciences in Nový Knín. The cross-sectional dimensions of the wind

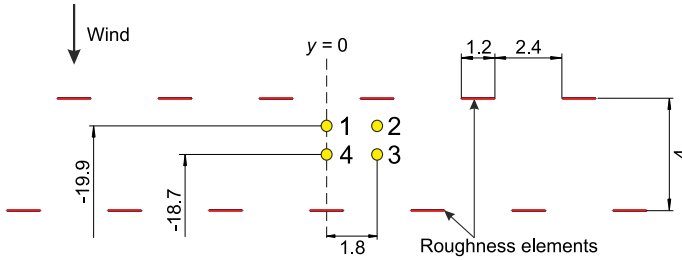


Fig. 3 Top view of the positions where the measurements of the approach boundary-layer vertical profiles were measured. The positions are related to the origin of the measurement coordinate system (x, y, z) and are normalized by the constant building height H of reference canyon model M1

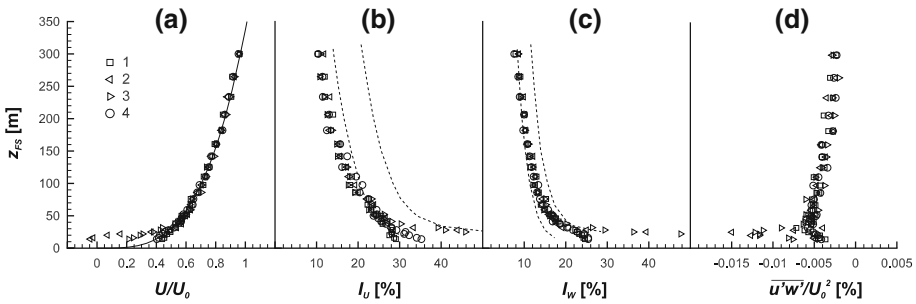


Fig. 4 Approach boundary-layer vertical profiles at full scale (1:400 wind-tunnel scale) of **a** the dimensionless longitudinal velocity component, **b** the longitudinal turbulent intensity, **c** the vertical turbulent intensity and **d** the dimensionless momentum flux at four positions among the roughness elements. *Solid line* power fit of the velocity profile for position 4; *dashed lines* upper and lower bounds of the turbulent intensity for very rough terrain recommended by VDI (2000)

tunnel were $1.5 \text{ m} \times 1.5 \text{ m}$ and the lengths of the development and test sections were 20.5 and 2 m, respectively. Throughout the measuring campaign, the wind-tunnel freestream velocity was maintained at $U_0 \approx 6.2 \text{ m s}^{-1}$ and measured using a Prandtl tube at a fixed position in the centre of the wind tunnel, 4 m upwind from the test section. The freestream velocity provides a Reynolds number for buildings that is sufficiently high ($Re_B \approx 24,400$, with respect to the reference height H) to fulfil the Reynolds number independence ($Re_{crit} = 11,000$) recommended by Snyder (1981).

A fully turbulent boundary layer formed at the bottom of the development section owing to turbulence generators and roughness elements at the beginning and along the remaining part of the development section, respectively. The approach boundary-layer characteristics were obtained employing two-dimensional laser Doppler anemometry (LDA), using a DANTEC BSA F-60 burst processor, at four positions between the roughness elements upwind from the model. The positions are described in detail in Fig. 3. Vertical profiles of the mean dimensionless longitudinal velocity component (U/U_0), longitudinal and vertical turbulent intensity (I_u and I_w , respectively) and dimensionless momentum flux ($\overline{u'w'}/U_0^2$) for all measurement positions are depicted in Fig. 4a–d, respectively. The best fit for all simulated boundary-layer parameters, as required by VDI (2000) guidelines for very rough terrain, is attained using vertical profiles from position 4 (circles in Fig. 4). Other profiles show higher discrepancy at full-scale heights $z_{FS} < 50 \text{ m}$ because they are close to the roughness elements (Fig. 3). Representative parameters of the mean longitudinal velocity vertical profile

Table 1 Boundary-layer parameters (where h is the mean height of buildings)

	z_0 (m)	d_0/h	α
Exp	1.87	0.12	0.27
VDI	0.5–2.0	0.75	0.24–0.40

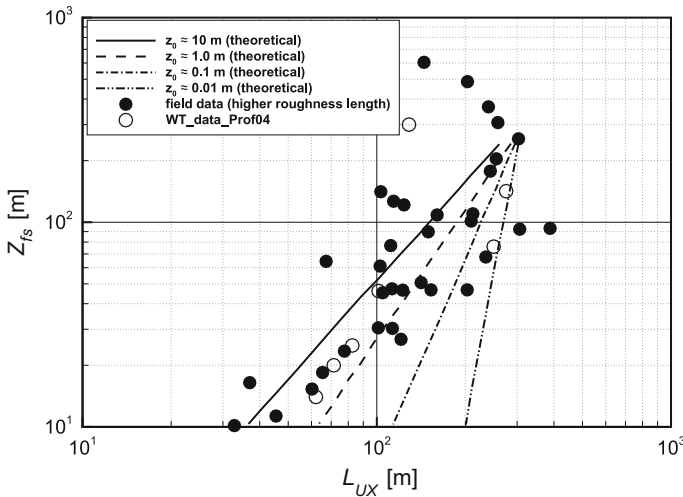


Fig. 5 Comparison of integral length scales, L_{ux} , between the present study (*open circles*) and field data for very rough terrain (*filled circles*) according to Counihan (1975) at different heights. The lines represent theoretical values of L_{ux} for appropriate roughness length z_0

(Fig. 4a) are presented at full scale in Table 1 in comparison with those recommended by VDI (2000) for very rough terrain. The mean roughness length z_0 and displacement d_0 were fitted by a logarithmic law and the power exponent α by a power law. All parameters, except d_0 , are within the limits recommended by VDI (2000) guidelines for the atmospheric boundary layer above very rough terrain. The displacement d_0 corresponds more to moderately rough terrain, which is more typical for suburban areas and might be acceptable for the presented urban-like array models. The same can be stated for the longitudinal turbulent intensity, I_u , at full-scale height $z_{FS} > 100$ m (Fig. 4b). However, below this level, where the street canyons are presented, I_u is within the limits for very rough terrain. The vertical turbulent intensity profiles of position 4, I_w (circles in Fig. 4c), are within the bounds recommended by VDI for the entire boundary-layer depth ($\delta_{FS} = 300$ m). The profiles of the dimensionless momentum flux $\overline{u'w'}/U_0^2$ have almost constant values with respect to height for $50 < z_{FS} < 100$ m (Fig. 4d).

The integral length scales of the streamwise velocity component, L_{ux} , calculated from time series measured at different heights across the boundary-layer depth, are compared with those from field measurements (Counihan 1975) over very rough terrain in Fig. 5. The theoretical values of L_{ux} for appropriate roughness length z_0 are also plotted. It is seen that the measured approach boundary layer at position 4 (open circles) has integral length scales within the theoretical values for very rough terrain (between solid and dashed lines), and in good accordance with field measurements (filled circles) for heights $z_{FS} < 50$ m.

2.3.2 Measurement Techniques

Ventilation processes within the street canyons were investigated by making simultaneous point measurements of the two velocity components (longitudinal and vertical) and concentration employing an LDA probe and an HFR400 fast-response flame ionization detector (FFID) manufactured by Cambustion Ltd., respectively. This simultaneous use of an LDA probe and FFID probe and was introduced by [Carpentieri et al. \(2012\)](#) and [Kukacka et al. \(2012\)](#). However, the experimental principle of the simultaneous point measurement of the velocity component and concentration was applied earlier by, e.g., [Fackrell and Robins \(1982\)](#), using thermo-anemometry instead of the optical method for velocity measurements.

The LDA and FFID probes were assembled together on a 3D traverser system that allowed the measuring volume of the LDA to be close to the intake of the FFID sampling tube, the latter being placed 1 mm above, 1 mm behind and 1 mm beside the centre of the LDA measuring volume. We performed several test measurements with different positions of both probes and confirmed a negligible effect of the FFID sampling tube on the LDA measurement. The LDA sampling frequency, depending on the investigated flow region, was maintained between 1 and 2 kHz during the whole measuring campaign. The FFID sampling frequency was set to 0.5 kHz, corresponding to its tested response time of 2 ms. Because the FFID sample tube had a diameter of 0.3 mm and length of 200 mm, the mean delay in the physical sampling time relative to LDA was approximately 12 ms. This time delay varied with air density and dynamic pressure at the measuring point. We thus used the maximum coefficient of correlation between the time series of the velocity component and concentration to obtain a more precise individual FFID time delay (ranging from 10 to 13 ms). The effect of LDA seeding particles (approximately $1 \mu\text{m}$ in diameter) on the FFID concentration measurements was corrected in the application of the FFID calibration method. For this, we measured separately the background concentration of LDA seeding particles and subtracted it from the measured concentration of the calibration gas (all without the running of the line source).

3 Results

Because the dominant pollutant exchange between the street canyon and external flow takes place in the vertical direction, in the case of perpendicular flow, we performed the simultaneous point measurements of each canyon model ($M1_R$, $M1_L$, M2 and M3) in two horizontal planes. The first plane was chosen at a dimensionless height $z/H = 0.6$ according to the lowest canyon wall (where the pitched roofs were not considered). This measurement area thus encloses each canyon from the top. The second plane at $z/H = 1$ was chosen as the reference height, where stronger effects of the variability of building height of models M2 and M3 on ventilation processes can be observed (Fig. 1b). Each plane had the same measuring grid of 5×13 points in the $x \times y$ directions (i.e., streamwise \times spanwise). At $z/H = 0.1$, we measured only the concentration in the windward and leeward wall regions, each consisting of 2×13 points, owing to LDA measuring constraints. Each canyon therefore had $(5 \times 13 \times 2) + (2 \times 13 \times 2) = 182$ measuring points. Consequently, the whole experiment consisted of $182 \times 4 \times 2 = 1456$ points (*number of points for each canyon \times number of canyons \times number of wind directions*) in total. According to the results of velocity and concentration central moment independence tests, the sampling time for

each measuring point was set to 120 s. The overall measurement error of pollution fluxes [considering the errors of velocity (1 %) and concentration measurements (4 %) and the positioning error of the 3D traverser system (1 %)] was estimated using ensemble statistics as 4.5 %.

3.1 Mean Flow and Concentration

Although the local differences between the flows and concentrations are hidden by means of their line averaging (Fig. 6), they are presented at first to compare the models from an integral point of view. The line averaging of the given variable V (denoted by angular brackets) was performed along the spanwise direction of the street canyon y (index j) for each streamwise position x (index i) and height of the measured plane z (index k) as

$$\langle V \rangle_{i,k} = \frac{\sum_{j=1}^N V_j}{N}, \tag{1}$$

where $N = 13$ is the number of points measured in the spanwise direction.

To present the variance of the variable along the spanwise direction of the canyon, vertical bars indicating the standard error of line averaging, $\sigma_{\bar{V}_i}$, are also plotted; these were computed as

$$\sigma_{\bar{V}_{i,k}} = \sqrt{\frac{\sum_{j=1}^N (V_j - \langle V \rangle_{i,k})^2}{N(N-1)}}. \tag{2}$$

The dimensionless concentration was obtained according to VDI (2000) guidelines as

$$C^* = \frac{CL_s U_{\text{ref}} H}{Q}, \tag{3}$$

where C is the measured mean concentration, L_s is the length of the line-source unit, U_{ref} is the reference velocity magnitude measured above the model centre at $z/H = 6$ and Q is the volume rate of ethane flow from the line source.

From a qualitative perspective, we observed very high similarity between the contour plots of the mean dimensionless streamwise and vertical velocity components, and dimensionless concentration fields of the right ($M1_R$) and left ($M1_L$) canyons (not shown here). However, to quantify the similarity, we calculated the mean percentage of the difference between the variables of $M1_R$ and $M1_L$ as

$$\Delta V = 100 \frac{1}{N} \sum_{i=1}^N \frac{|V_{R,i} - V_{L,i}|}{\frac{|V_{R,i} + V_{L,i}|}{2}}, \tag{4}$$

where $V_{R,i}$ and $V_{L,i}$ are the particular mean values of the dimensionless variable corresponding to position i of $M1_R$ and $M1_L$ measurement grids, respectively, and N is the number of positions across the measured horizontal plane for the given case. $\Delta V = 0$ implies that the models are in ideal agreement for a given variable and case.

The mean percentages of the differences for each variable and perpendicular wind direction are listed in Table 2. For both heights, the agreement is very good except in the case of the vertical velocity ($\Delta W/U_{\text{ref}}$). The overall higher values of $\Delta W/U_{\text{ref}}$, are due to small average values (on the order of 0.001) in comparison with the absolute differences in Eq. 4. The streamwise distributions of the line-averaged dimensionless longitudinal velocity component (U/U_{ref}), vertical velocity (W/U_{ref}) and concentration (C^*) across each canyon model are compared in Fig. 6a–c, respectively.

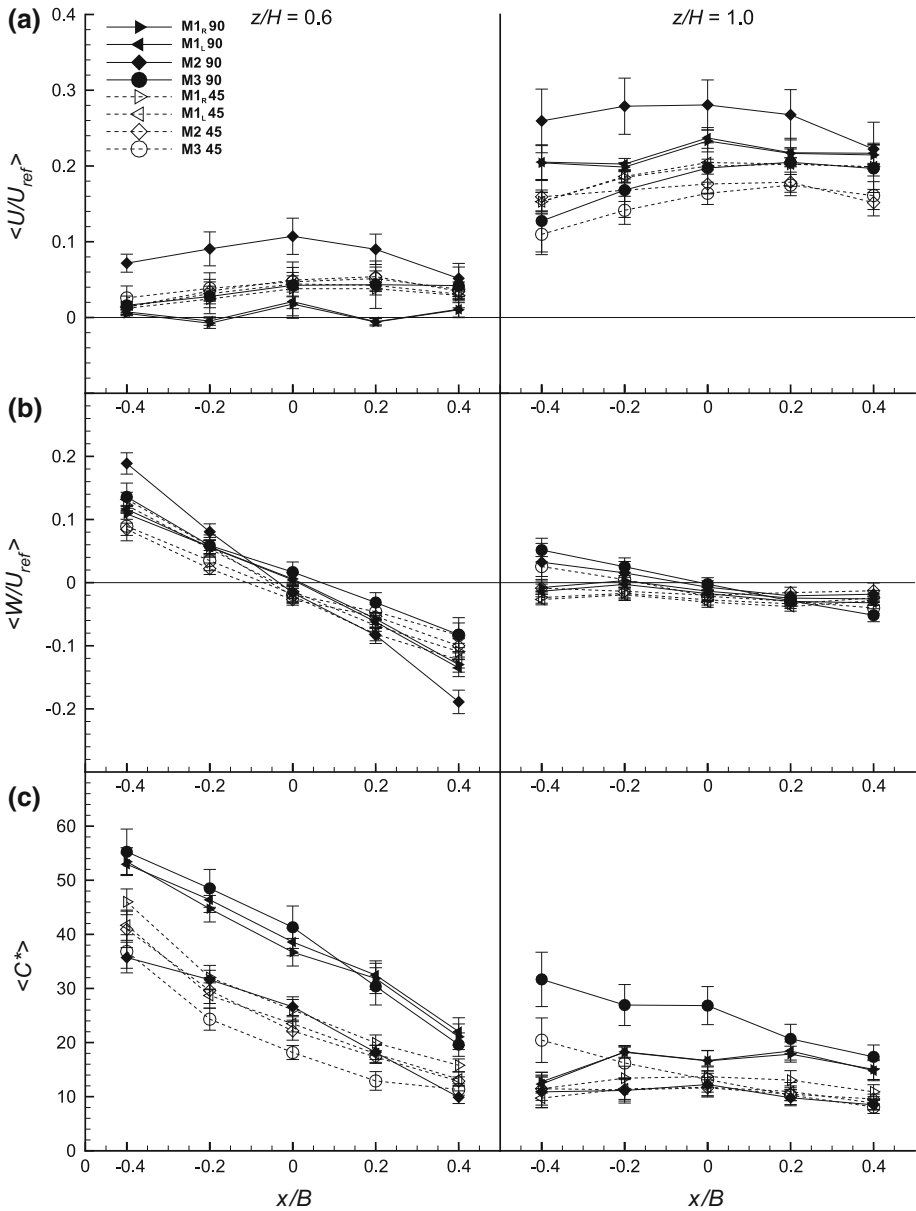


Fig. 6 Streamwise distribution of the mean dimensionless **a** longitudinal and **b** vertical velocity components, and **c** concentration, line-averaged along the spanwise direction of the canyon. *Right triangles* model $M1_R$; *left triangles* model $M1_L$; *diamonds* model $M2$; *circles* model $M3$; *filled symbols* perpendicular wind direction; *open symbols* oblique wind direction; *left column* $z/H = 0.6$; *right column* $z/H = 1$. The vertical bars indicate standard error of the averaged variable and the line source is positioned at $x/B = 0$

Model $M3$ (circles), representing on average the step-down canyon, has similar line-averaged values (velocities and concentration) as the symmetrical model $M1$ (triangles) in the case of the perpendicular wind direction at height $z/H = 0.6$. The results for canyon

Table 2 Similarity between models $M1_R$ and $M1_L$ expressed as the mean percentage of difference between the mean dimensionless variables for the perpendicular wind direction and two investigated heights (where zero refers to ideal similarity)

Height	$\Delta U/U_{ref}$	$\Delta W/U_{ref}$	ΔC^*
$z/H = 0.6$	11.5	30.3	2.0
$z/H = 1$	0.8	25.8	0.3

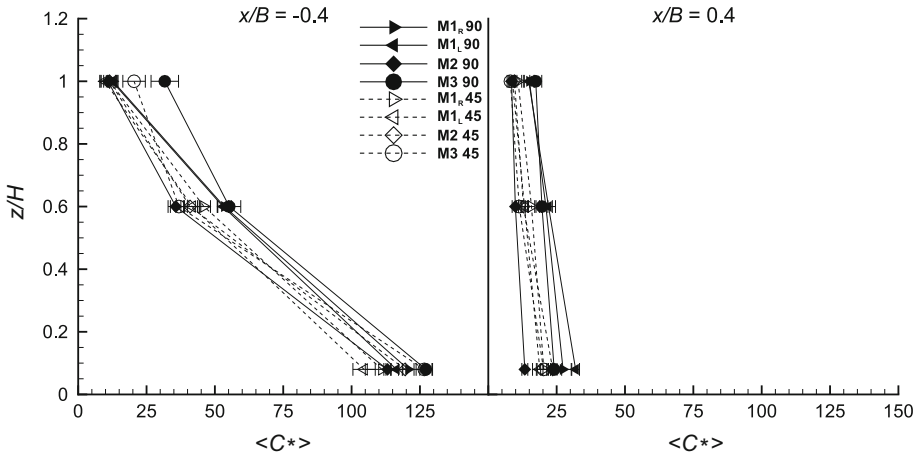


Fig. 7 Mean dimensionless concentration vertical profiles line-averaged along the spanwise direction of the canyon at $x/B = -0.4$ (left column) and $x/B = 0.4$ (right column) walls. The symbols have the same meaning as those in Fig. 6. The horizontal bars indicate the standard error of the line-averaged concentration

M2 (diamonds), representing on average the step-down canyon, differ from those of M1 and M3 appreciably. The line-averaged concentrations of M2 are lower than those of M3 and M1 by a factor of approximately 1.5 across the entire canyon width at height $z/H = 0.6$ (Fig. 6c). This is in agreement with the results of previous wind-tunnel and CFD studies (Hoydysh and Dabberdt 1988; Xie et al. 2006). However, the presented concentration levels do not support the finding of Hoydysh and Dabberdt (1988) that the concentration on the windward ($x/B = 0.4$) side of the step-down canyon is higher than that on the leeward side ($x/B = -0.4$). The main explanation is that there are different local roof-height arrangements along each canyon wall, as will be later demonstrated for concentration and pollution flux fields. The main effect of the roof-height arrangement of model M2 is that it produces the highest line-averaged velocities (both streamwise and vertical) and the lowest concentration levels across the whole canyon width for each investigated height. The line-averaged vertical concentration profiles along the leeward and windward walls (Fig. 7) have appreciably lower values for model M2 also at the pedestrian level ($z/H = 0.1$).

For the oblique wind direction (open symbols in Fig. 6), there are negligible variations of line-averaged velocities ($\langle U/U_{ref} \rangle$, $\langle W/U_{ref} \rangle$) among all compared street canyon models ($M1_R$, $M1_L$, M2 and M3). This might be attributed to the channelling effects producing more uniform flow within all canyons. A weaker but still strong recirculation vortex can be seen at $z/H = 0.6$ (open symbols in Fig. 6b). The centre of the vortex with respect to the streamwise coordinates coincides with the canyon centre ($x/B = 0$) as demonstrated

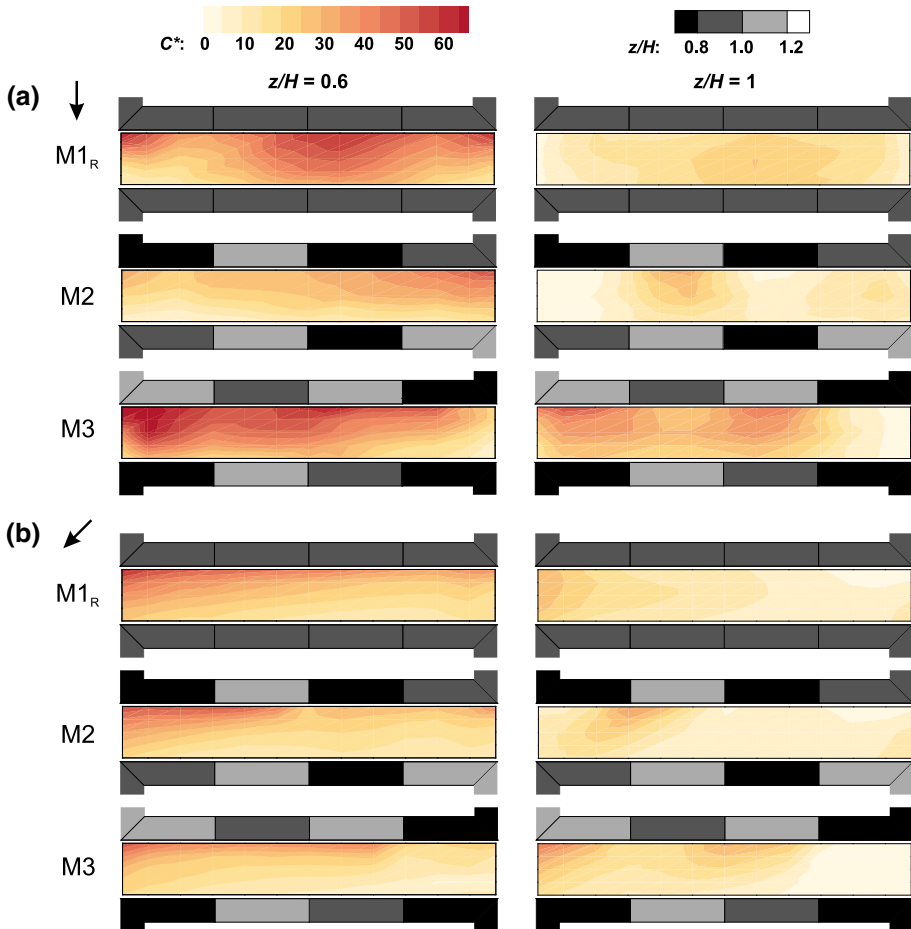


Fig. 8 Mean dimensionless concentration fields C^* (coloured contours) for **a** perpendicular, and **b** oblique wind directions, all canyon models (rows) and dimensionless heights (columns). The roof height along the appropriate canyon wall is represented by dimensionless height z/H (grey contours)

for all investigated heights and flow directions. The strongest line-averaged upward and downward air motions along the leeward ($x/B = -0.4$) and windward ($x/B = 0.4$) walls, respectively, arise in the case of model M2 at $z/H = 0.6$ for the oblique wind direction (open diamonds in Fig. 6b). This suggests that the averaged step-up canyon configuration produces a stronger vortex inside the street canyon. At $z/H = 1$, the upward and downward motion is weaker for canyon models with varying roof height (M2 and M3) compared with the case when $z/H = 0.6$. In the case of the model with constant roof height (M1_R and M1_L), where $z/H = 1$ for the roof level along the entire canyon, this air motion practically diminishes.

A strong effect of the wind direction on the mean concentration, $\langle C^* \rangle$, is observed for all canyon models in Fig. 6c and can be more clearly seen in mean dimensionless concentration fields presented in Fig. 8. If the flow direction changes from perpendicular to oblique, the concentration field levels decrease appreciably for each canyon model. While the concentration contours for model M1_R have a symmetrical spatial distribution at both heights in the case

of the perpendicular wind direction (Fig. 8a, first row), models M2 and M3 produce asymmetrical concentration fields (second and third rows in Fig. 8a). These are strongly affected by local roof-height arrangements along both canyon walls of models M2 and M3. The line-averaged concentrations for the oblique wind direction show that the averaged step-down model (M3) has the lowest values among all canyon models across the whole canyon width at $z/H = 0.6$ (open circles in Fig. 6c, left column). This is in contrast with the case of the perpendicular wind direction for which the highest concentration levels within model M3 are presented by means of line-averaged values (filled circles in Fig. 6c) and concentration fields (Fig. 8a, third row). Owing to the locally lowest roof ($z/H = 0.8$) along the leeward and windward walls being positioned at the right margin of the model M3, cleaner air penetrates the canyon in the case of the oblique wind direction (Fig. 8b, third row). Hence, for a proper investigation of the spatial concentration distribution within a fully 3D canyon, the spanwise distribution of the roof height along both canyon walls needs to be taken into account. This stresses the importance of the street-canyon three-dimensionality (geometrical variability in all directions) in realistic dispersion studies.

3.2 Analysis of Ventilation Processes

3.2.1 Pollution Fluxes

Analysis of the vertical pollution fluxes provides insight into the ventilation processes occurring within the street canyons. We computed the mean turbulent pollution flux from synchronized time series of the vertical velocity and concentration using the eddy-correlation method defined by Stull (1988) as

$$\overline{c^{*'}w'} = \frac{1}{N} \sum_{i=1}^n c^{*'}_i w'_i, \tag{5}$$

where $c^{*'}$ and w'_i are the fluctuations of the dimensionless concentration and vertical velocity at a particular time, respectively, and N is the length of the discrete time series. The mean total pollution flux was calculated as the sum of its turbulent and advective parts,

$$\overline{c^*w} = \overline{c^{*'}w'} + C^*W, \tag{6}$$

where C^* and W are the temporally-averaged dimensionless concentration and vertical velocity, respectively. The relative contribution of the turbulent pollution flux to the total vertical pollution flux was computed as

$$\overline{c^{*'}w'}_{\text{rel}} = \frac{|\overline{c^{*'}w'}|}{|\overline{c^{*'}w'}| + |C^*W|}. \tag{7}$$

If $\overline{c^{*'}w'}_{\text{rel}} = 1$, all pollution transport is produced by the turbulent contribution. We applied line averaging (Eq. 1) and computed the standard error estimation (Eq. 2) for pollution fluxes and we present them in dimensionless form (by dividing them by reference velocity U_{ref}).

The line-averaged values of the dimensionless total pollution flux, $\langle \overline{c^*w}/U_{\text{ref}} \rangle$, show very strong upward and not so strong downward (re-emission) total pollutant transport at the leeward and windward walls, respectively, for the perpendicular wind direction at $z/H = 0.6$ of all canyon models (Fig. 9a, left column). At $z/H = 1$, $\langle \overline{c^*w}/U_{\text{ref}} \rangle$ points upward across the whole canyon width of each canyon model (Fig. 9a, right column). No appreciable effect of the wind direction on total pollutant transport is observed in the case of the model with constant roof height ($M1_R$ and $M1_L$), while there is an appreciable decrease in total

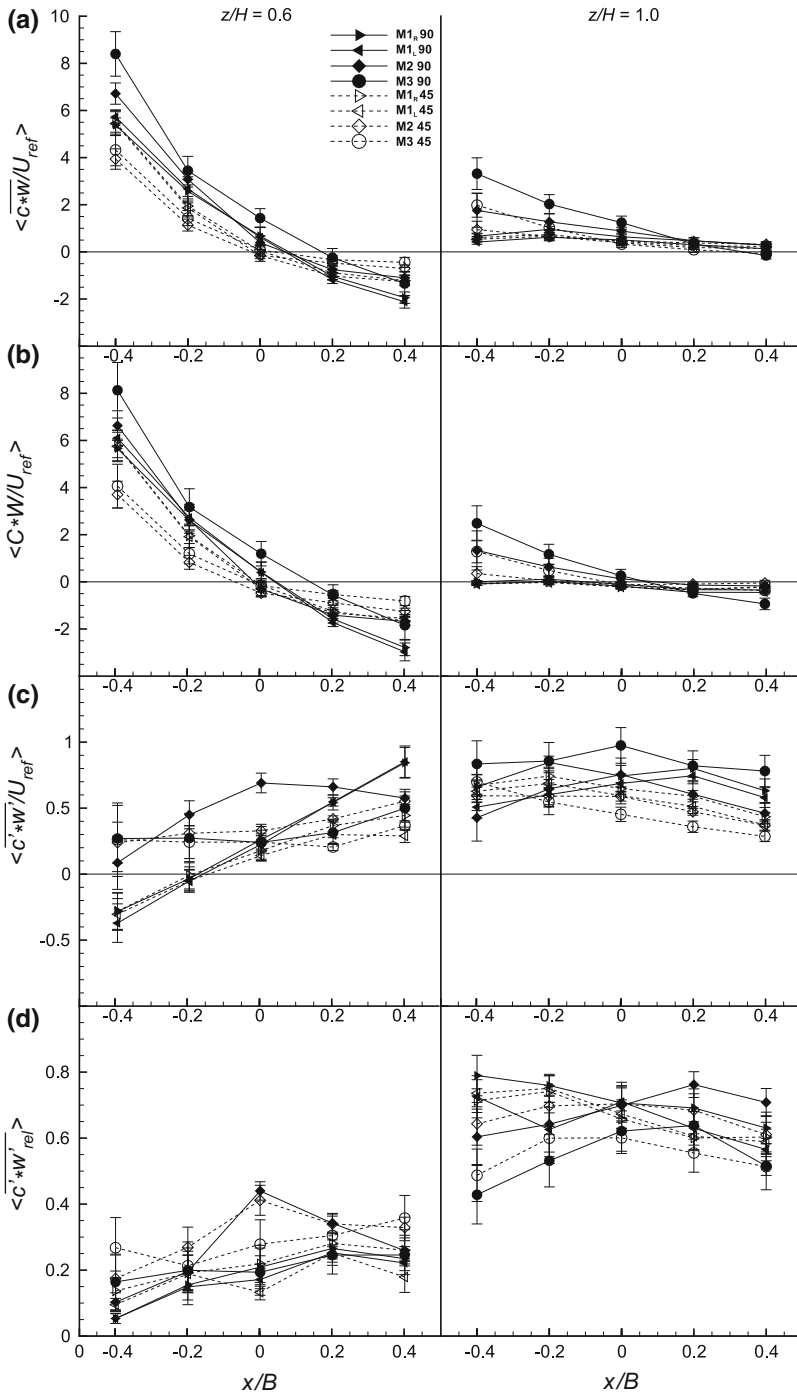


Fig. 9 Streamwise distributions of the pollution fluxes line-averaged along the spanwise direction of the canyon: **a** total, **b** advective and **c** turbulent; **d** relative contribution of the turbulent pollution flux to total pollution flux. The symbols have the same meaning as in Fig. 6

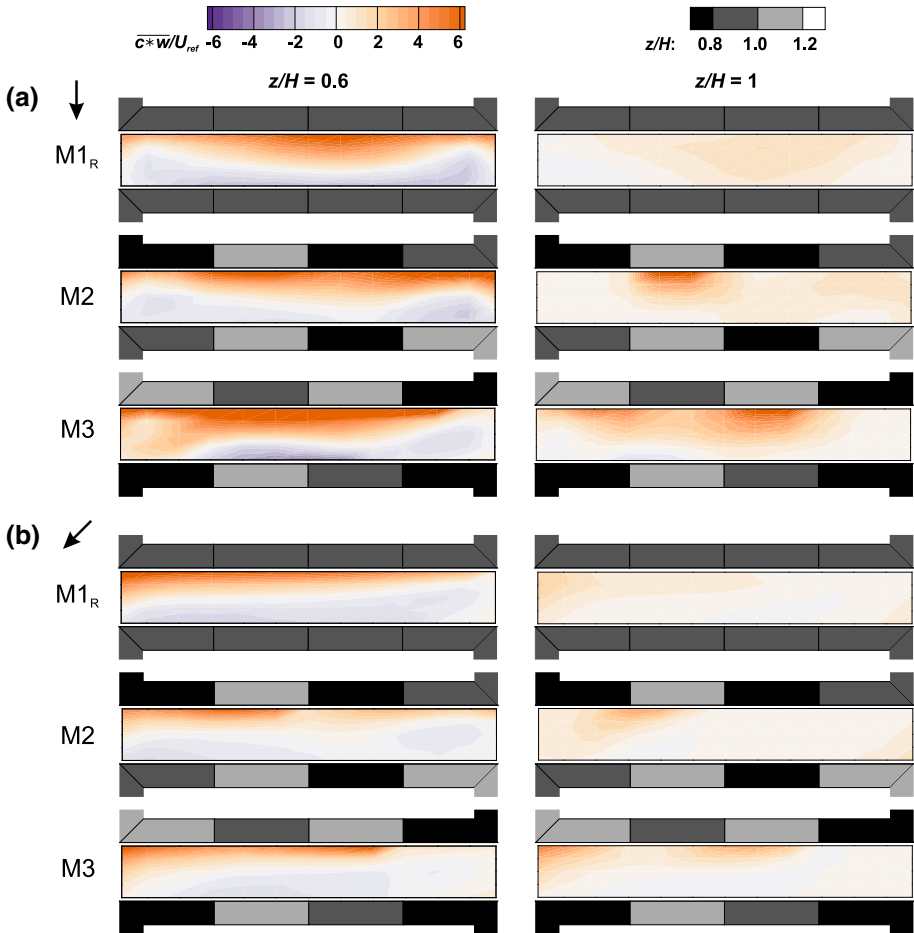


Fig. 10 Mean dimensionless total pollution flux fields $\langle c^*w \rangle / U_{ref}$ (coloured contours) for, **a** perpendicular, and **b** oblique wind directions, all canyon models (rows) and dimensionless heights (columns). The roof height along the appropriate canyon wall is represented by dimensionless height z/H (grey contour)

pollutant transport for models with varying roof height if the wind direction changes from perpendicular to oblique. The strongest upward pollutant transport was observed for model M3 at both heights in the case of the perpendicular wind direction (filled circles in Fig. 9a, first column). In the case of the oblique wind direction, the strongest upward pollutant transport and re-emission were achieved with the model having constant roof height at $z/H = 0.6$ (open triangles in Fig. 9a, first column).

As for the mean velocity and concentration fields, the local variability of the total pollution flux is lost in the line-averaged horizontal profiles. While model M2 shows similar symmetry of the $\langle c^*w \rangle / U_{ref}$ field as model M1_R at $z/H = 0.6$ (Fig. 10a, left column), the effect of different building heights on the field can be clearly seen for $z/H = 1$ (Fig. 10a, right column). Owing to the presence of only one highest building on the canyon leeward side, higher pollution fluxes are produced by model M2 than by M1_R. Especially, in the case of model M3, the strongest upward total pollution fluxes at both investigated heights (Fig. 10a,

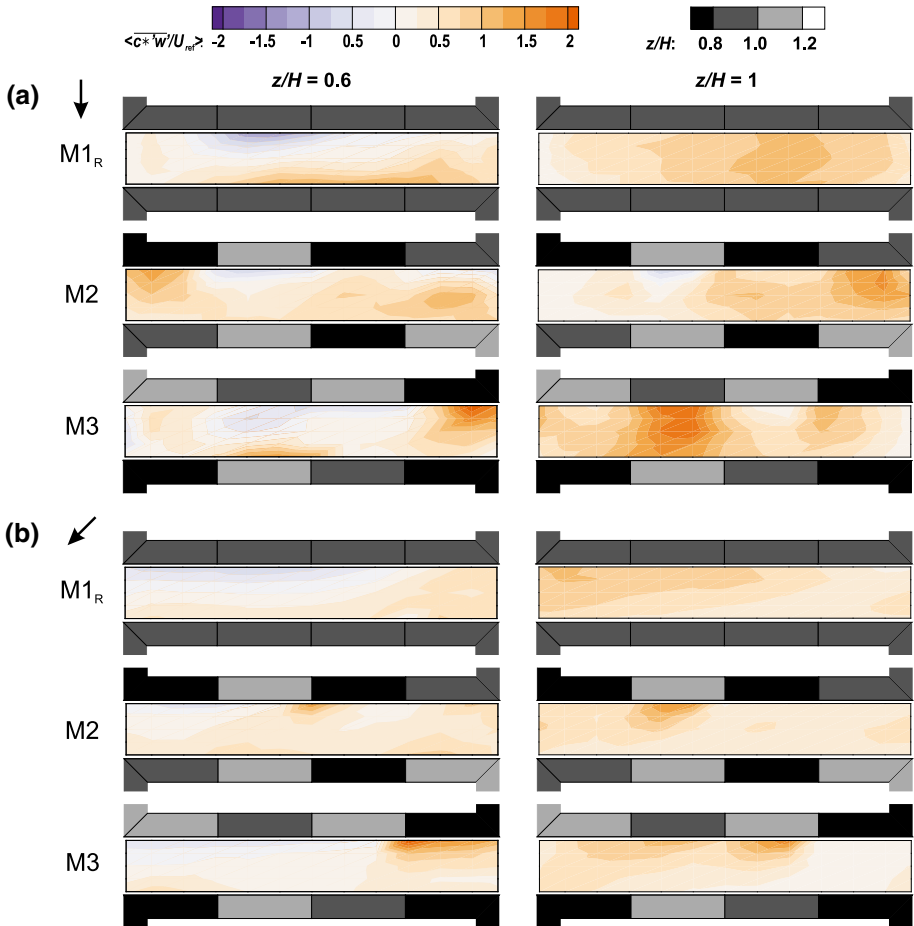


Fig. 11 Mean dimensionless turbulent flux fields $\overline{c^*w'}/U_{\text{ref}}$ (coloured contours) for, **a** perpendicular, and **b** oblique wind directions, all canyon models (rows) and dimensionless heights (columns). The roof height along the appropriate canyon wall is represented by dimensionless height z/H (grey contour)

third row) are enhanced by the presence of the two highest buildings along the leeward side. The spatial variability of the total pollution flux for all models is more complex in the case of the oblique wind direction (Fig. 10a) and remains hidden when looking only at the line-averaged horizontal profiles.

The effects of the type of street canyon on the line-averaged advective pollution flux, $\langle C^*W/U_{\text{ref}} \rangle$, and turbulent pollution flux, $\langle \overline{c^*w'}/U_{\text{ref}} \rangle$, are shown in Fig. 9b, c, respectively. Within ($z/H = 0.6$) canyons of constant roof height (M1_R and M1_L), the turbulent pollution transport opposes the advective pollution transport as reported in our previous study (Kukacka et al. 2014). The same cannot be stated for the models with varying roof height (M2 and M3), where the line-averaged turbulent pollution fluxes are positive across the whole canyon width, irrespective of height (Fig. 9b, left and right columns). This is again the consequence of line averaging, while the contour plots show the interchanging of negative and positive turbulent fluxes along the leeward walls of both canyon models M2 and M3 at both investigated heights

(Fig. 11a). This confirms that the roof-height variability along the canyon walls needs to be considered in studying local pollutant transport patterns within realistic 3D canyons.

The contribution of the turbulent pollution flux to the total pollution flux, $\langle c^{*'}w'_{rel} \rangle$, is dominant at $z/H = 1$ for all canyon models and is strongly affected by the model type and is independent of the wind direction even if the line averaging is taken into account (Fig. 9d, right column). The spatial averaging of the turbulent flux contribution fields (not shown here) at $z/H = 1$ for each type of model, M1_R, M2 and M3, results in contributions of 72, 69 and 57 %, respectively, in the case of the perpendicular wind direction. Michioka et al. (2014), using an LES model, computed almost the same value of $\langle c^{*'}w'_{rel} \rangle = 75 \%$ at the roof level of a 3D canyon with flat roofs and $L/B = 4$ as in our case of model M1_R (72 %).

3.2.2 Relative Pollutant Removal

To better understand the mechanisms of pollutant removal acting within the street canyons, we calculated the relative pollutant removal from the mean total pollution flux fields as

$$E_{rel} = \frac{1}{Q} \int_{-0.4B}^{0.4B} \int_{0.02L}^{0.98L} \overline{cw} dy dx, \tag{8}$$

where \overline{cw} is the total vertical pollution flux and Q is the rate of emission from the source presented in the canyon of the same length (L). Owing to the complexity of the three-dimensionality of the flow within the canyons, together with the finite length of the line source, we performed the integration only in the case of the perpendicular wind direction at height $z/H = 0.6$. This height ensures that all canyon models are enclosed by the measurement plane from the top. Of course, that area did not cover the entire horizontal area owing to spatiality constraints of the measurement (integral limits in Eq. 8). Therefore, the integrated (measurement) plane corresponded to 77 % of the total area enclosed by the canyon geometry in the case of the height $z/H = 0.6$; $E_{rel} = 1$ implies that all emissions from the source are removed through the measurement plane to the flow aloft.

Integrating the mean dimensionless concentration pollution field, C^* (Fig. 8), across the measurement plane and dividing it by its area, A , we obtain the spatially-averaged dimensionless concentration at a given height,

$$\langle C^* \rangle = \frac{1}{A} \int_{-0.4B}^{0.4B} \int_{0.02L}^{0.98L} C^* dy dx. \tag{9}$$

As in the case of E_{rel} , we integrate C^* only for the case of the perpendicular wind direction at height $z/H = 0.6$. Results for E_{rel} and $\langle C^* \rangle$ are presented in Table 3. This shows that the pollutant removal ($E_{rel} = 0.63$) from the middle canyon height to the flow aloft in the case of the constant roof-height model (M1_R) is similar to that in the case of the canyon with flat roofs ($E_{rel} = 0.65$) calculated by Michioka et al. (2014). Approximately 37 % (35 % in the

Table 3 Relative pollutant removal, E_{rel} , and spatially-averaged dimensionless concentration, $\langle C^* \rangle$, for each canyon model at height $z/H = 0.6$ and for the perpendicular wind direction

	M1 _R	M2	M3
E_{rel}	0.63	0.84	1.31
$\langle C^* \rangle$	37.5	24.4	40.3

case of Michioka et al. 2014) of the pollutant is emitted laterally to the intersections, and pitched roofs of constant height do not appreciably affect pollutant removal from the canyon.

Canyons with variable roof heights (M2 and M3) have higher relative pollutant removals to the top and hence less removal laterally. Striking pollutant removal mechanisms occur in the case of model M3 ($E_{rel} = 1.31$), where not only all emission from the source is removed but another 31 % of this emission is ventilated from the canyon surroundings. The dimensionless total pollution flux fields presented in Fig. 10a clearly show that this extra pollutant entrainment occurs at the left edge of canyon M3, where the biggest step-down local configuration is presented. This yields the highest spatially-averaged dimensionless concentration of model M3 ($\langle C^* \rangle = 40.3$) and cannot be attributed to the higher re-emission rates, in contrast to the case of the 2D street-canyon models as was demonstrated by, e.g., Liu et al. (2005). From the point of view of E_{rel} and $\langle C^* \rangle$, model M3 might be determined as the most unfavourable street-canyon arrangement according to the simulated line-source model. Meanwhile, if only the line source within the canyon is simulated, model M3 has better ventilation processes than model M1_R owing to the extra unpolluted air lateral entrainment from the intersections, hence reducing $\langle C^* \rangle$ from 40.3 to 28.2. This suggests that additional pollutant fluxes through the lateral areas of the canyon need to be experimentally investigated in future work to gain better insight into the mechanisms of pollutant removal from the 3D canyon. The best ventilation performance is, without any considerations, achieved by M2 with respect to the highest E_{rel} and the lowest $\langle C^* \rangle$ among all investigated canyon models.

3.2.3 Relationship Between the Dominant Momentum and Scalar Fluxes

For the atmospheric surface layer, it is widely accepted that coherent structures, referred to as the sweep and ejection of momentum, are responsible for the mass transport (Katul et al. 2006; Li and Bou-Zeid 2011). We thus also focused on street-canyon ventilation with respect to the relationships between the dominant events of the momentum and pollution fluxes. We used a simple conditional technique known as *quadrant analysis*, developed by Willmarth (1975), which is applied to scatter plots of two turbulent quantities. Here, we used instantaneous longitudinal (u') and vertical (w') velocity fluctuations for the momentum flux, and the dimensionless concentration ($c^{*'}$) and vertical (w') fluctuations for the scalar flux.

We follow Katul et al. (2006) and use the same quadrant nomenclature for the momentum transport (Fig. 12a). The meaning of physical processes of defined events are as follows: faster particles of air are transported downwards during sweep events. Meanwhile, ejection refers to the transport of slower particles upwards. Prevailing sweep and ejection events in a turbulent flow within the boundary layer are caused by the transport of momentum towards

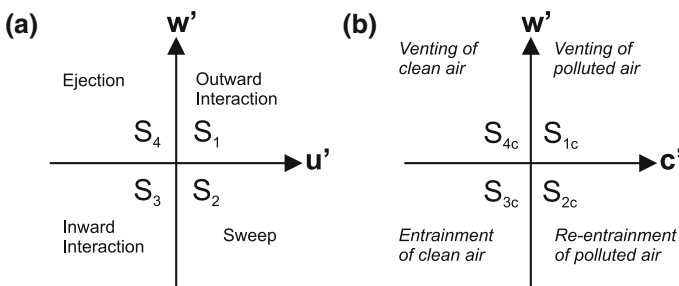


Fig. 12 Schema of the quadrant nomenclature for, **a** momentum, and **b** scalar transport

a surface. Outward and inward interactions transport faster moving particles upwards and slower particles downwards, respectively.

For scalar transport, we design the quadrant nomenclature according to the processes going on (Fig. 12b). The first and third quadrants, where the venting of polluted air ($c' > 0$ and $w' > 0$) and the entrainment of clean air ($c' < 0$ and $w' < 0$) take place, respectively, are considered as street-canyon ventilation processes. The remaining second and fourth quadrants represent the re-entrainment of polluted air ($c' > 0$ and $w' < 0$) and venting of clean air ($c' < 0$ and $w' > 0$), respectively, and are thus considered pollution processes.

We found that sweeps and ejections and ventilation processes are dominant in all simulated cases. Hence, we present only their fractional contributions, which we computed as

$$S_i = \frac{|\langle \overline{u'w'} \rangle_i|}{|\overline{u'w'}|}, S_{ic} = \frac{|\langle \overline{c'w'} \rangle_i|}{|\overline{c'w'}|}, \tag{10a}$$

$$\langle \overline{u'w'} \rangle_i = \frac{1}{T} \int_0^T u'(t)w'(t)I_i dt, \tag{10b}$$

$$\langle \overline{c'w'} \rangle_i = \frac{1}{T} \int_0^T w'(t)c'(t)I_i dt, \tag{10c}$$

where $\langle \rangle$ is the conditional average, $\overline{u'w'}$ and $\overline{c'w'}$ are the momentum and scalar fluxes, respectively, and I is the indicator function. $I_i = 1$ if $u'w'$ (or $c'w'$) is within quadrant $i = 2, 4$ (or 1,3) and $I_i = 0$ otherwise.

The streamwise distributions of the line-averaged fractional contributions of sweeps (S_2) and ejections (S_4), and the entrainment of clean air (S_{1c}) and venting of polluted air (S_{3c}) at $z/H = 1$ are presented in Fig. 13a–d, respectively. The sweeps (Fig. 13a) contribute more than the ejections (Fig. 13b) across the whole canyon, irrespective of the street-canyon model. This shows that the prevailing mechanism of the momentum transport is a motion of faster moving air downwards into the canyon. Interestingly, there is no appreciable effect of the wind direction on sweep and ejection streamwise distributions for any canyon model.

If we look at the ventilation processes in the case of the perpendicular wind direction, models M1 and M2 have higher contributions to polluted air ventilation (filled triangles and diamonds in Fig. 13d, respectively) than to the entrainment of the clean air (Fig. 13c). The ventilation processes are approximately equal for model M3 (filled circles in Fig. 13c and d). The highest polluted air ventilation and the lowest clean-air entrainment among all investigated canyons are observed for model M2, across the entire canyon width. If the wind direction becomes oblique, an appreciable increase in polluted air ventilation is observed for each canyon model (open symbols in Fig. 13d). The same cannot be stated for clean-air entrainment, where only one appreciable increase (model M2) occurs (open diamonds in Fig. 13d).

To quantify the relationship between the coherent structures and ventilation processes, we calculated the coefficients of correlation between the sweep and clean-air entrainment ($r_{2,3c}$) and between the ejection and polluted air ventilation ($r_{4,1c}$) as

$$r_{2,3c} = \frac{\overline{(u'w')_2(w'c')_3}}{\sigma_{uw2}\sigma_{wc3}}, \tag{11a}$$

$$r_{4,1c} = \frac{\overline{(u'w')_4(w'c')_1}}{\sigma_{uw4}\sigma_{wc1}}, \tag{11b}$$

where $(u'w')_i$ and $(w'c')_j$ are the time series of the momentum ($i = 2, 4$) and scalar events ($j = 3, 1$), respectively, and σ_{uwi} and σ_{wcj} are their standard deviations. Similar coefficients

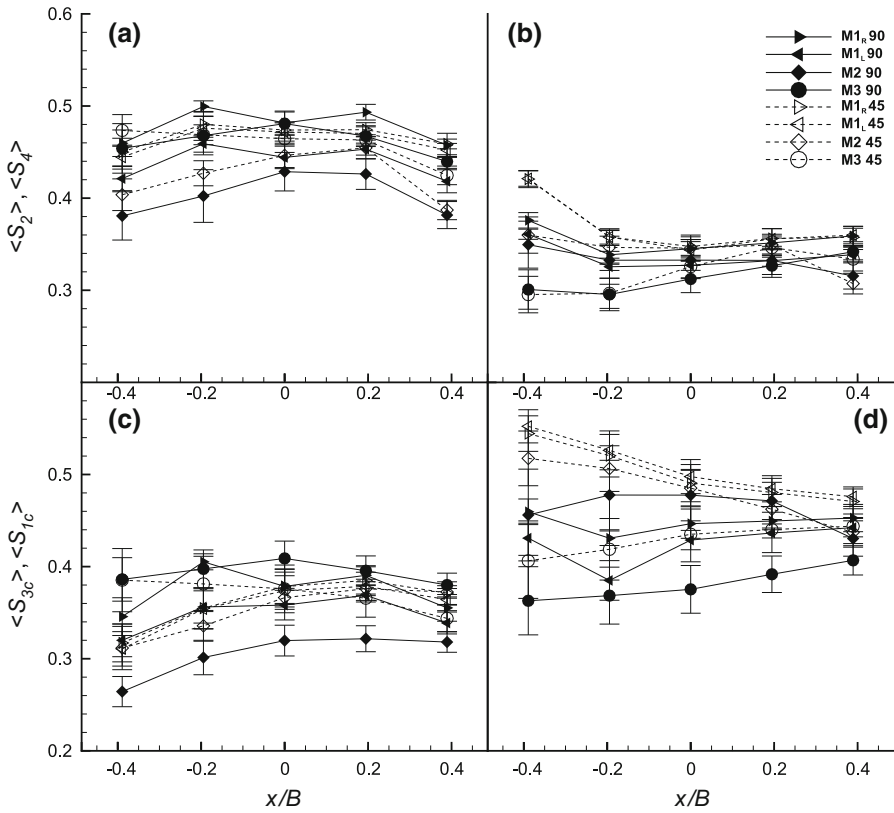


Fig. 13 Fractional contributions of the, **a** sweep (S_2), **b** ejection (S_4), **c** entrainment of clean air (S_{3c}), and **d** venting of the polluted air (S_{1c}), line-averaged along the spanwise direction at height $z/H = 1.0$. The symbols have the same meaning as in Fig. 6

of correlation between the momentum flux and two scalar fluxes (sensible and latent heat) were used by Li and Bou-Zeid (2011).

Because events are always negative and the scalar fluxes are always positive, the correlation coefficient is always negative. We thus present the absolute values of the correlation coefficients to stress that the investigated dominant momentum (sweeps and ejections) and scalar (inward and outward interactions) fluxes vary in the same direction.

The line-averaged streamwise distributions of $|\overline{r_{2,3c}}|$ and $|\overline{r_{4,1c}}|$ at both investigated heights are presented in Fig. 14a, b, respectively. First, there is little effect of the wind direction on either correlation coefficient in all investigated cases. Very high correlations (ranging from 0.7 to 0.75) between sweeps and clean-air entrainment ($|\overline{r_{2,3c}}|$) are seen across all canyon model widths at $z/H = 1.0$ for both wind directions (Fig. 14a, right column). This finding supports the idea that the sweep events “sweep” the clean air into the canyon at roof level. At $z/H = 0.6$, lower but still appreciable correlations between sweeps and clean-air entrainment are observed for canyons with varying roof height.

The correlations between the ejection and polluted air ventilation ($|\overline{r_{4,1c}}|$) are weak at both heights. However, they are still appreciable at $z/H = 1.0$ (Fig. 14b, right column). This

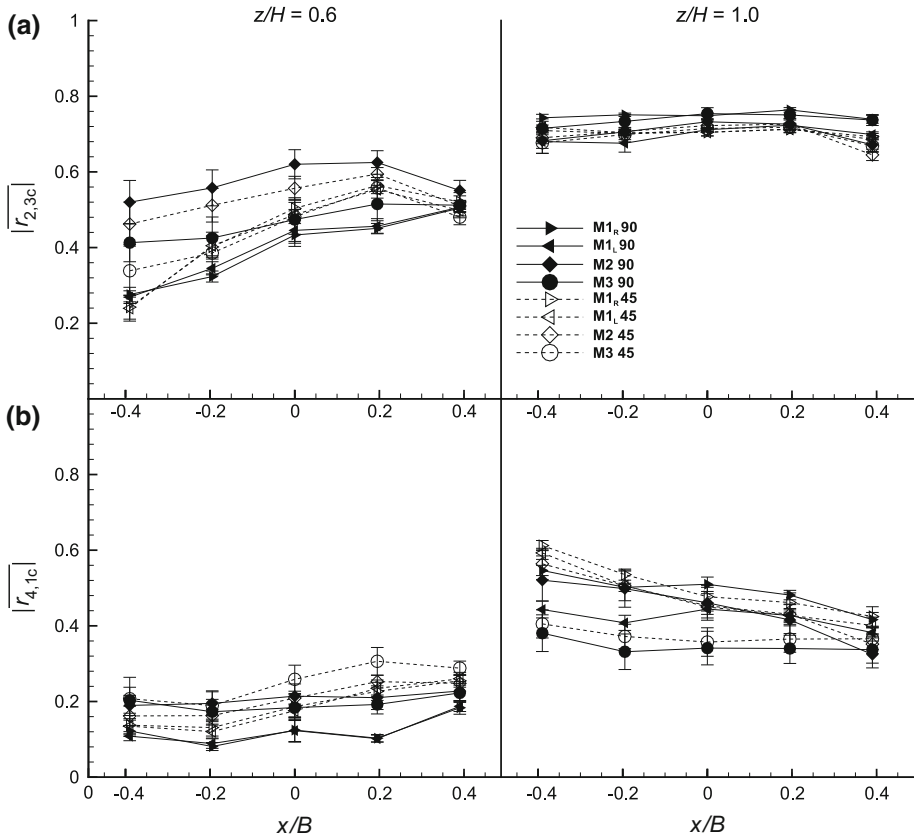


Fig. 14 Streamwise distributions of the coefficients of correlation between **a** sweep and clean air entrainment $|r_{2,3c}|$, and between **b** ejection and polluted air venting $|r_{4,1c}|$, line-averaged along the spanwise direction of the canyon. The *symbols* have the same meaning as in Fig. 6

supports the results of CFD studies (e.g., Michioka et al. (2014), Liu et al. (2015)), where the low momentum fluid ($u' < 0$) was related to pollutant removal at roof level ($z/H = 1$).

4 Conclusions

According to topical knowledge of street-canyon ventilation obtained in previous wind-tunnel and CFD studies, we designed a wind-tunnel experiment that addressed ground-level line-source ventilation processes within 3D street canyons. The three-dimensionality refers to roof-height non-uniformity along both leeward and windward canyon walls. We simulated two approach flow directions over three different types of street-canyon models arranged in an urban-like array and formed by courtyard-type buildings.

Detailed analysis of the mean velocity, concentration and pollution flux fields shows that roof-height variability along both canyon walls cannot be treated as that of an averaged step-up, step-down or uniform street canyon if one needs to study the ventilation processes within the canyon locally or for non-perpendicular approach wind directions. However, the

studied non-uniform street canyons, represented as averaged step-up and step-down canyons, produce lower and higher concentration levels than the uniform canyon, respectively, in the case of a perpendicular wind direction.

We demonstrated the complexity of the flow three-dimensionality within non-uniform canyons by analyzing the pollutant removal for the perpendicular wind direction. Generally, more pollutant is removed to the flow aloft from the non-uniform canyons than from the uniform canyon. In the case of the averaged step-down canyon, not only were all the emissions from the line source positioned within the canyon removed but also another 31 % of this emission amount was ventilated from the canyon surroundings. Hence, the resulting highest spatially-averaged concentration cannot be attributed to the higher pollutant re-emission as was demonstrated in many CFD studies on 2D canyons.

If only the line source within the canyon is taken into account, the averaged step-down canyon will have better ventilation than the uniform canyon owing to the extra lateral entrainment of unpolluted air from the intersections. The best ventilation performance with respect to the highest pollutant removal and the lowest spatially-averaged concentrations, and hence the lowest re-emission, was achieved by the averaged step-up canyon. To gain better insight into the mechanisms of pollutant removal from 3D canyons, additional experimental and numerical studies are needed.

We introduced nomenclature for the ventilation processes according to quadrant analysis of the pollutant flux. We observed that the venting of polluted air from a canyon increases if the wind direction changes from perpendicular to oblique, irrespective of the studied canyon model. Furthermore, we found strong correlations between the turbulent coherent structures and ventilation processes at roof level, irrespective of the canyon model and wind direction. The sweeps and ejections were highly correlated (>0.5) with clean air entrainment and polluted air venting, respectively.

Acknowledgments This work was supported by the Charles University in Prague (project GAUK No. 535412), the Czech Science Foundation GACR (project GAP101/12/1554 and GAP15-18964S) and the institutional support RVO: 61388998.

References

- Addepalli B, Pardyjak ER (2014) A study of flow fields in step-down street canyons. *Environ Fluid Mech*. doi:[10.1007/s10652-014-9366-z](https://doi.org/10.1007/s10652-014-9366-z)
- Baik JJ, Kim JJ (2002) On the escape of pollutants from urban street canyons. *Atmos Environ* 36(3):527–536. doi:[10.1016/S1352-2310\(01\)00438-1](https://doi.org/10.1016/S1352-2310(01)00438-1)
- Baik JJ, Park RS, Chun HY, Kim JJ (2000) A laboratory model of urban street-canyon flows. *J Appl Meteorol* 39(9):1592–1600. doi:[10.1175/1520-0450\(2000\)039<1592:ALMOUS>2.0.CO;2](https://doi.org/10.1175/1520-0450(2000)039<1592:ALMOUS>2.0.CO;2)
- Barlow JF, Harman IN, Belcher SE (2004) Scalar fluxes from urban street canyons. Part 1: Laboratory simulation. *Boundary-Layer Meteorol* 113:369–385
- Belcher SE (2005) Mixing and transport in urban areas. *Philos Trans Roy Soc A* 363(October):2947–2968. doi:[10.1098/rsta.2005.1673](https://doi.org/10.1098/rsta.2005.1673)
- Bezpalcova K (2006) Physical modelling of flow and diffusion in urban canopy. PhD thesis, Charles University in Prague, Prague
- Blackman K, Perret L, Savory E (2015) Effect of upstream flow regime on street canyon flow mean turbulence statistics. *Environ Fluid Mech* 15(4):823–849. doi:[10.1007/s10652-014-9386-8](https://doi.org/10.1007/s10652-014-9386-8)
- Blocken B (2015) Computational fluid dynamics for urban physics: importance, scales, possibilities, limitations and ten tips and tricks towards accurate and reliable simulations. *Build Environ* 91:219–245. doi:[10.1016/j.buildenv.2015.02.015](https://doi.org/10.1016/j.buildenv.2015.02.015)
- Britter RE, Hanna SR (2003) Flow and dispersion in urban areas. *Annu Rev Fluid Mech* 35(1):469–496. doi:[10.1146/annurev.fluid.35.101101.161147](https://doi.org/10.1146/annurev.fluid.35.101101.161147)

- Cai XM, Barlow JF, Belcher SE (2008) Dispersion and transfer of passive scalars in and above street canyons—large-eddy simulations. *Atmos Environ* 42(23):5885–5895. doi:[10.1016/j.atmosenv.2008.03.040](https://doi.org/10.1016/j.atmosenv.2008.03.040)
- Carpentieri M, Robins AG (2015) Influence of urban morphology on air flow over building arrays. *J Wind Eng Ind Aerodyn* 145:61–74. doi:[10.1016/j.jweia.2015.06.001](https://doi.org/10.1016/j.jweia.2015.06.001)
- Carpentieri M, Hayden P, Robins AG (2012) Wind tunnel measurements of pollutant turbulent fluxes in urban intersections. *Atmos Environ* 46:669–674. doi:[10.1016/j.atmosenv.2011.09.083](https://doi.org/10.1016/j.atmosenv.2011.09.083)
- Cheng H, Castro IP (2002) Near-wall flow development after a step change in surface roughness. *Boundary-Layer Meteorol* 105(August 2001):411–432. doi:[10.1023/A:1020355306788](https://doi.org/10.1023/A:1020355306788)
- Counihan J (1975) Adiabatic atmospheric boundary layer: a review and analysis of data from period 1880–1972. *Atmos Environ* 9(10):871–905
- Dabberdt WF (1991) Street canyon dispersion: sensitivity to block shape and entrainment. *Atmos Environ* 25:11431153
- Fackrell JE, Robins AG (1982) Concentration fluctuations and fluxes in plumes from point sources in a turbulent boundary layer. *J Fluid Mech* 117:26
- Grimmond CSB, Oke TR (1999) Aerodynamic properties of urban areas derived from analysis of surface form. *J Appl Meteorol* 38(9):1262–1292. doi:[10.1175/1520-0450\(1999\)038<1262:APOUAD>2.0.CO;2](https://doi.org/10.1175/1520-0450(1999)038<1262:APOUAD>2.0.CO;2)
- Gu ZL, Zhang YW, Cheng Y, Lee SC (2011) Effect of uneven building layout on air flow and pollutant dispersion in non-uniform street canyons. *Build Environ* 46(12):2657–2665. doi:[10.1016/j.buildenv.2011.06.028](https://doi.org/10.1016/j.buildenv.2011.06.028)
- Hoydysh GW, Dabberdt FW (1988) Kinematics and dispersion characteristics of flows in asymmetric street canyons. *Atmos Environ* 22:2677–2689
- Hoydysh G W, Griffiths A R, Ogawa Y (1974) A scale model study of the dispersion of pollution in street canyons. In: 67th annual meeting of the Air Pollution Control Association
- Huang YD, He WR, Kim CN (2015) Impacts of shape and height of upstream roof on airflow and pollutant dispersion inside an urban street canyon. *Environ Sci Pollut Res* 22(3):2117–2137. doi:[10.1007/s11356-014-3422-6](https://doi.org/10.1007/s11356-014-3422-6)
- Kastner-Klein P, Plate E (1999) Wind-tunnel study of concentration fields in street canyons. *Atmos Environ* 33(24–25):3973–3979. doi:[10.1016/S1352-2310\(99\)00139-9](https://doi.org/10.1016/S1352-2310(99)00139-9)
- Kastner-Klein P, Berkowicz R, Britter R (2004) The influence of street architecture on flow and dispersion in street canyons. *Meteorol Atmos Phys* 87(1–3):121–131. doi:[10.1007/s00703-003-0065-4](https://doi.org/10.1007/s00703-003-0065-4)
- Katul G, Poggi D, Cava D, Finnigan J (2006) The relative importance of ejections and sweeps to momentum transfer in the atmospheric boundary layer. *Boundary-Layer Meteorol* 120:367–375. doi:[10.1007/s10546-006-9064-6](https://doi.org/10.1007/s10546-006-9064-6)
- Klein P, Leidl B, Schatzmann M (2007) Driving physical mechanisms of flow and dispersion in urban canopies. *Int J Climatol* 27(September):1887–1907. doi:[10.1002/joc.1581](https://doi.org/10.1002/joc.1581)
- Kukacka L, Nosek S, Kellnerova R, Jurcakova K (2012) Wind tunnel measurement of turbulent and advective scalar fluxes: a case study on intersection ventilation. *Sci World J* 381:357. doi:[10.1100/2012/381357](https://doi.org/10.1100/2012/381357)
- Kukacka L, Fuka V, Nosek S, Kellnerova R, Janour Z (2014) Ventilation of idealised urban area, LES and wind tunnel experiment. *EPJ Web Conf* 62:1–10. doi:[10.1051/epjconf/20146702062](https://doi.org/10.1051/epjconf/20146702062)
- Leidl BM, Meroney RN (1997) Car exhaust dispersion in a street canyon: numerical critique. *J Wind Eng Ind Aerodyn* 67:293–304
- Li D, Bou-Zeid E (2011) Coherent structures and the dissimilarity of turbulent transport of momentum and scalars in the unstable atmospheric surface layer. *Boundary-Layer Meteorol* 140(2):243–262. doi:[10.1007/s10546-011-9613-5](https://doi.org/10.1007/s10546-011-9613-5)
- Liu CH, Leung DYC, Barth MC (2005) On the prediction of air and pollutant exchange rates in street canyons of different aspect ratios using large-eddy simulation. *Atmos Environ* 39:1567–1574. doi:[10.1016/j.atmosenv.2004.08.036](https://doi.org/10.1016/j.atmosenv.2004.08.036)
- Liu CH, Ng CT, Wong CC (2015) A theory of ventilation estimate over hypothetical urban areas. *J Hazard Mater* 296:9–16
- Louka P, Belcher SE, Harrison RG (2000) Coupling between air flow in streets and the well-developed boundary layer aloft. *Atmos Environ* 34(16):2613–2621. doi:[10.1016/S1352-2310\(99\)00477-X](https://doi.org/10.1016/S1352-2310(99)00477-X)
- Madalozzo DMS, Braun AL, Awruch AM, Morsch IB (2014) Numerical simulation of pollutant dispersion in street canyons: geometric and thermal effects. *Appl Math Model* 38(24):5883–5909. doi:[10.1016/j.apm.2014.04.041](https://doi.org/10.1016/j.apm.2014.04.041)
- Meroney RN, Pavageau M, Rafailidis S, Schatzmann M (1996) Study of line source characteristics for 2-D physical modelling of pollutant dispersion in street canyons. *J Wind Eng Ind Aerodyn* 62:37–56
- Michioka T, Takimoto H, Sato A (2014) Large-Eddy simulation of pollutant removal from a three-dimensional street canyon. *Boundary-Layer Meteorol* 150:259–275. doi:[10.1007/s10546-013-9870-6](https://doi.org/10.1007/s10546-013-9870-6)

- Moon K, Hwang JM, Kim BG, Lee C, Ji Choi (2014) Large-eddy simulation of turbulent flow and dispersion over a complex urban street canyon. *Environ Fluid Mech* 14(6):1381–1403
- Nelson MA, Pardyjak ER, Klewicki JC, Pol SU, Brown MJ (2007) Properties of the wind field within the Oklahoma City Park Avenue street canyon. Part I: Mean flow and turbulence statistics. *J Appl Meteorol Clim* 46(12):2038–2054. doi:[10.1175/2006JAMC1427.1](https://doi.org/10.1175/2006JAMC1427.1)
- Nozu T, Tamura T (2012) LES of turbulent wind and gas dispersion in a city. *J Wind Eng Ind Aerodyn* 104–106:492–499
- Perret L, Savory E (2013) Large-Scale structures over a single street canyon immersed in an urban-type boundary layer. *Boundary-Layer Meteorol* 148(1):111–131. doi:[10.1007/s10546-013-9808-z](https://doi.org/10.1007/s10546-013-9808-z)
- Rafailidis S (1997) Influence of building areal density and roof shape on the wind characteristics above a town. *Boundary-Layer Meteorol* 85(2):255–271. doi:[10.1023/A:1000426316328](https://doi.org/10.1023/A:1000426316328)
- Rafailidis S, Schatzmann M (1995) Concentration measurements with different roof patterns in street canyons with aspect ratios $B/H=1/2$ and $B/H=1$. Technical report, Meteorology Institute, University of Hamburg, Hamburg
- Robins A, Scaperdas A, Savory E, Savory E, Grigoriadis D, Scaperdas A, Robins A, Grigoriadis D (2002) Spatial variability and source-receptor relations at a street intersection. *Water Air Soil Poll Focus* 2(5):381–393. doi:[10.1023/A:1021360007010](https://doi.org/10.1023/A:1021360007010)
- Salizzoni P, Marro M, Soulhac L, Grosjean N, Perkins JR (2011) Turbulent transfer between street canyons and the overlying atmospheric boundary layer. *Boundary-Layer Meteorol* 141(3):393–414. doi:[10.1007/s10546-011-9641-1](https://doi.org/10.1007/s10546-011-9641-1)
- Savory E, Perret L, Rivet C (2013) Modelling considerations for examining the mean and unsteady flow in a simple urban-type street canyon. *Meteorol Atmos Phys* 121(1–2):1–16. doi:[10.1007/s00703-013-0254-8](https://doi.org/10.1007/s00703-013-0254-8)
- Schatzmann M, Leitl B (2011) Issues with validation of urban flow and dispersion CFD models. *J Wind Eng Ind Aerodyn* 99(4):169–186. doi:[10.1016/j.jweia.2011.01.005](https://doi.org/10.1016/j.jweia.2011.01.005)
- Snyder WH (1981) Guidelines for fluid modelling of atmospheric diffusion. EPA office of Air quality, USA
- Stull RB (1988) *An Introduction to Boundary Layer Meteorology*. Kluwer Academic Publishers, Dordrecht, 666 pp
- Takimoto H, Inagaki A, Kanda M, Sato A, Michioka T (2013) Length-scale similarity of turbulent organized structures over surfaces with different roughness types. *Boundary-Layer Meteorol* 147(2):217–236. doi:[10.1007/s10546-012-9790-x](https://doi.org/10.1007/s10546-012-9790-x)
- Theurer W (1999) Typical building arrangements for urban air pollution modelling. *Atmos Environ* 33(24–25):4057–4066. doi:[10.1016/S1352-2310\(99\)00147-8](https://doi.org/10.1016/S1352-2310(99)00147-8)
- VDI (2000) *Physical modelling of flow and dispersion processes in the atmospheric boundary layer—application of wind tunnels*. Verein Deutscher Ingenieure (VDI), Berlin
- Willmarth WW (1975) Structure of turbulence in boundary layers. *Arch Appl Mech* 15:159–254
- Xie X, Huang Z, Wang JS (2005) Impact of building configuration on air quality in street canyon. *Atmos Environ* 39(25):4519–4530. doi:[10.1016/j.atmosenv.2005.03.043](https://doi.org/10.1016/j.atmosenv.2005.03.043)
- Xie X, Huang Z, Wang J (2006) The impact of urban street layout on local atmospheric environment. *Build Environ* 41(10):1352–1363
- Yang Y, Shao Y (2008) Numerical simulations of flow and pollution dispersion in urban atmospheric boundary layers. *Environ Modell Softw* 23(7):906–921. doi:[10.1016/j.envsoft.2007.10.005](https://doi.org/10.1016/j.envsoft.2007.10.005)
- Zajic D, Fernando HJS, Brown MJ, Pardyjak ER (2015) On flows in simulated urban canopies. *Environ Fluid Mech* 15(2):275–303. doi:[10.1007/s10652-013-9311-6](https://doi.org/10.1007/s10652-013-9311-6)